Phased Arrays of Cavity–backed Antennas for 5G Smartphones with Metallic Casing

Miodrag Tasić, *Member IEEE* and Dragan Nikolić

***Abstract*—Cellular handset antennas for future 5G applications need to provide beam steering, so the antenna focus is on the phased arrays. For the metallic casing handsets, a cavity–backed antenna is a natural candidate for an element of the phased array. Cavity can be cut in the handset wall and filled with the dielectric, thus potential waterproofing can be maintained. Radiation is trough the cavity, hence the metallic casing is not an obstacle. In this paper we use electromagnetic models to investigate the problems and limitations of a phased array with cavity–backed antennas.**

***Index term*—5G; phased arrays; cavity–backed antenna; electromagnetic modeling.**

I. Introduction

IN order to provide higher bandwidths for cellular services, 5G technology will (also) use frequency bands near (28 GHz) or in (38 GHz, 60 GHz) millimeter–wave (mmWave) spectrum [1]. Since propagation losses in mmWave spectrum are higher than in the spectrum under 3 GHz (used so far, for 4G and older technologies), utilization of highly directive antennas with beam steering is implied. Frequency range around 28 GHz seems to be especially interesting, since minimum of propagation loss occurs in that range [2].

Design principles for 5G antennas are yet to be established [3]. However, for cellular handsets with metallic casing, antennas in the form of slots in the casing are one obvious solution [4], [5]. Namely, the metal casing would block the signal if the antenna was inside, hence typical phased array of patches cannot be used. In that sense, a cavity–backed antenna [6] is a good choice for the element of the phased array. At the time being, smartphones with 5G label have glass back panels and, furthermore, can be delivered without mmWave 5G antenna modules (though they have slots for this purpose). Anyway, phased arrays with cavity–backed elements can be naturally employed if a handset has a metal frame (if not full metallic casing).

In this work, we implement a phased array of cavity–backed antennas as in [4]. We adopt the same cavity size, aimed to work in the frequency range around 28 GHz, whereas we optimized dimensions of feeding microstrip lines. Two models of a cellular handset with phased arrays are discussed—one with a metallic frame, but without a cover, and the other with a metallic cover, i.e., with full metal casing. Interiors of models are empty. In reality, the casings are completely filled: the largest part is occupied by the battery (and, maybe, the coil for wireless charging), then by the camera and motherboards. More comprehensive study is necessary to consider effects of these components, which is beyond the scope of this work.

The geometrical and electromagnetic models of the phased array antenna are presented in Section II, numerical results are presented in Section III, whereas conclusions are given in Section IV.

Miodrag Tasić – Elektrotehnički fakultet, Univerzitet u Beogradu, Bulevar Kralja Aleksandra 73, 11020 Beograd, Srbija (e-mail: tasic@etf.rs).

Dragan Nikolić – Elektrotehnički fakultet, Univerzitet u Beogradu, Bulevar Kralja Aleksandra 73, 11020 Beograd, Srbija (e-mail: nikolicdragansiki@gmail.com).

II. Antenna Model

Outlines of the model are shown in Fig. 1. A cavity–backed antenna comprises a cavity excited by a stepped pin fed by a microstrip line. There are two eight–element phased arrays along two edges. Each cavity–backed antenna is enumerated. A 3D view, with the dimensions, is shown in the figure inset. The model is situated in the Cartesian coordinate system, also shown in the figure.

Cavity is shown in Fig. 2. It is excited by a metal stepped pin. The wider part of the pin is connected to the wall of the cavity, whereas the narrower part is soldered to the microstrip line. In the original design, the metal pin is nailed from outside of the metallic frame. In electromagnetic sense, these two models are equivalent. The pin is attached to the feeding microstrip line, as shown in Fig. 3. The point voltage generator is connected to the other side of the microstrip line, between the line and the ground plane.

Dimensions, in mm, are shown in Fig. 4 (*xy*–plane) and in Fig. 5 (*xz*–plane). Dimensions of the cavity and the stepped pin and the parameters of the dielectrics are the same as in [4]. The relative permittivity of the dielectric in the cavities is 3, whereas the relative permittivity and the thickness of the microstrip line substrate are 2.2, and 0.254 mm. The boards of the microstrip lines for different antennas are separated to achieve better isolation between the ports. The dimensions of the microstrip line and of all gaps around it are optimized to achieve good balance between port's reflection coefficients and the coupling between the ports. Note that the structure is sensitive in this regard, so one can expect a notable discrepancy between simulated and measured S–parameters.

Solid 3D model of the handset frame with the cavity–backed antennas is shown in Fig. 6. Since handset covers commonly are not metallic (or, at least, one of them is not), such model can be considered as an approximate model for the handset with low permittivity dielectric covers.

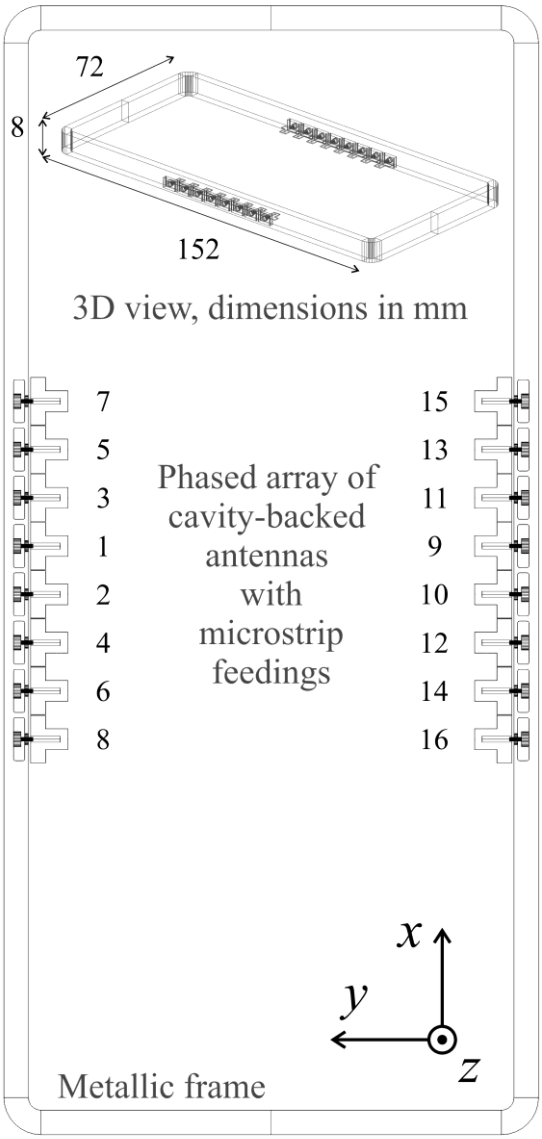

Fig. 1. Cellular handset metallic frame with two eight–element phased arrays with cavity–backed elements.

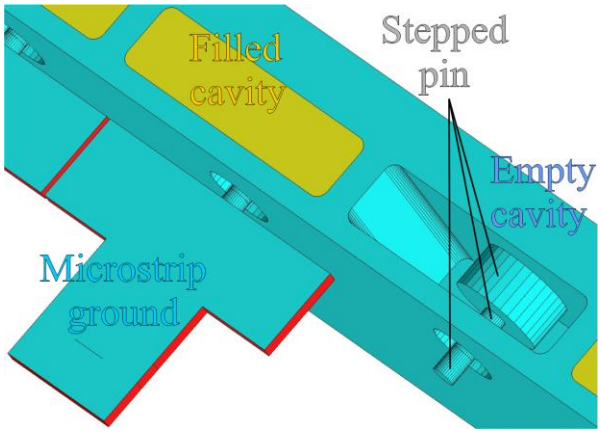

Fig. 2. Cavity filled with dielectric material and excited by a stepped pin. Empty cavity is shown as an illustration of the interior.

The handset with the metallic covers is shown in the Fig. 6 inset. The covers are model as infinitely thin metallic plates. The losses in the metal and dielectrics are neglected.

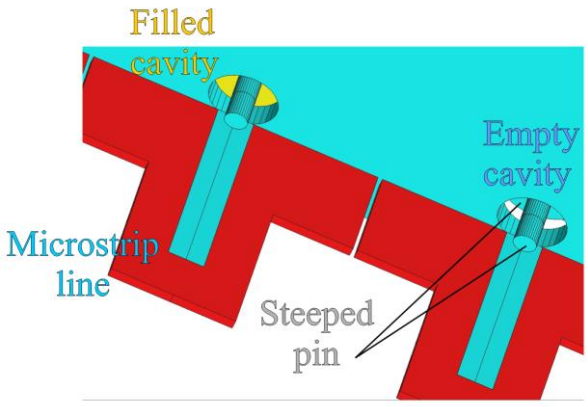

Fig. 3. Stepped pin fed by a microstrip line.

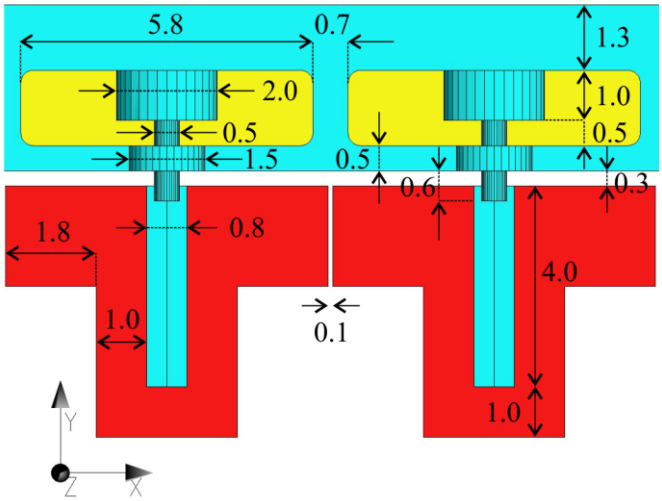

Fig. 4. Dimensions of the structure in mm, *xy*–plane.

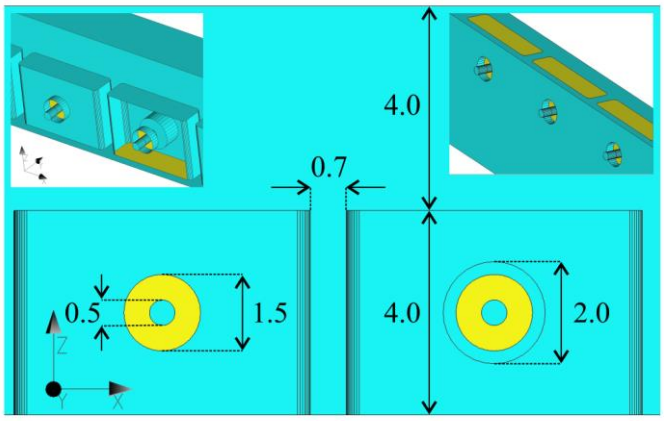

Fig. 5. Dimensions of the structure in mm, *xz*–plane. 3D views are shown in the figure insets.

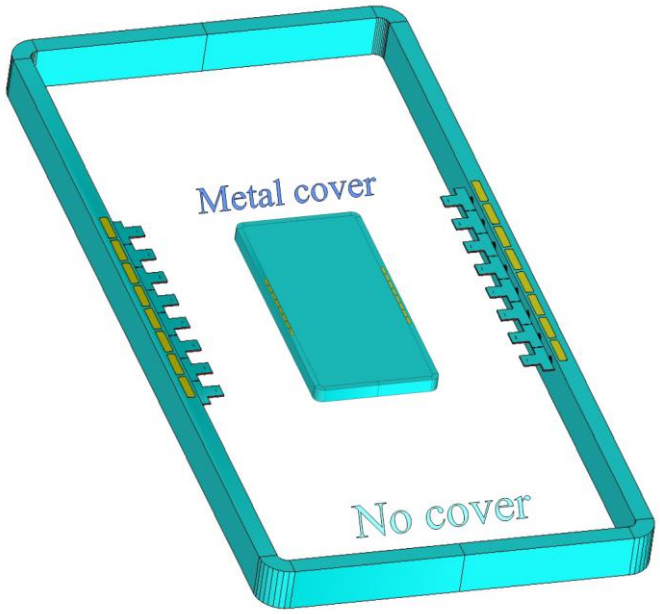

Fig. 6. Solid model of the handset frame, without the cover, with the cavities (in yellow). Model with the metallic cover is shown in the figure inset.

III. Numerical Results

All simulations are performed using the software for electromagnetic modeling WIPL-D [7]. S–parameters are calculated in 21 linearly spaced frequencies from 27 GHz to 29 GHz. Radiation is calculated at 28 GHz. From a few numerical simulations, it is concluded that losses in the metal and the dielectric are not significant factor, so the presented results are for the lossless materials. The ports are at the voltage generators positions. The feeder used for microstrip lines has low reflection coefficient, but de–embedding of S–parameters in the plane of interest may be necessary for ultimate precision. Simulations are performed using two models from Fig. 6, referenced as Metal cover and No cover.

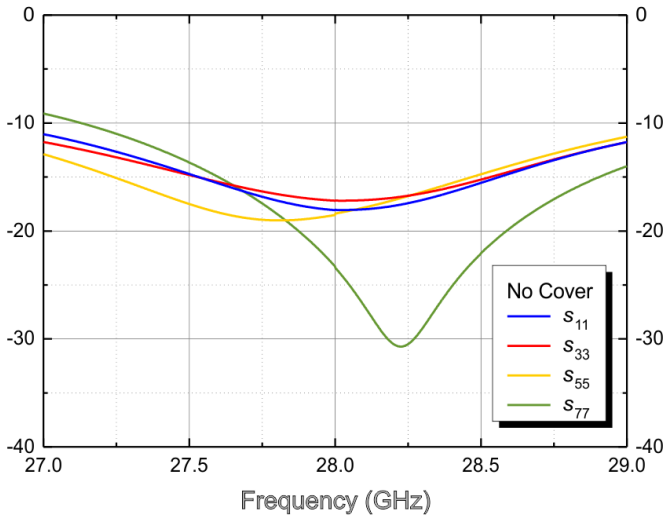

Fig. 7. Magnitudes of the reflection coefficients (i.e., magnitudes of S_{jj} parameters, in dB) at the ports 1, 3, 5, and 7, for the No cover model.

Magnitudes of the reflection coefficients (i.e., magnitudes of S_{jj} parameters, in dB) at the ports 1, 3, 5, and 7 (as numerated in Fig. 1), for No cover model, is shown in Fig. 7. Since the model is symmetric along two axes (x and y), every other port has a reflection coefficient equal to one of those in Fig. 7. Ports 1 and 3 have similar reflection, whereas reflection curves for ports 5 and 7 are shifted in frequency (about 250 MHz), down, i.e., up. Furthermore, reflection at port 1 reaches significantly lower magnitudes. The curves are smooth, and 10 dB bandwidth is excellent (> 2 GHz).

Magnitudes of the couplings (i.e., magnitudes of S_{jk} parameters, in dB) between some of the ports, for No cover model, is shown in Fig. 8. As expected, the coupling is stronger for physically closer ports. The most critical are pairs of adjacent ports at the end of the phased array (i.e., S_{75} has the highest magnitude of all), and generally ports at the end of the array has stronger couplings (e.g., S_{73} is higher than S_{51} and S_{41}). The curves are smooth, as in Fig. 7.

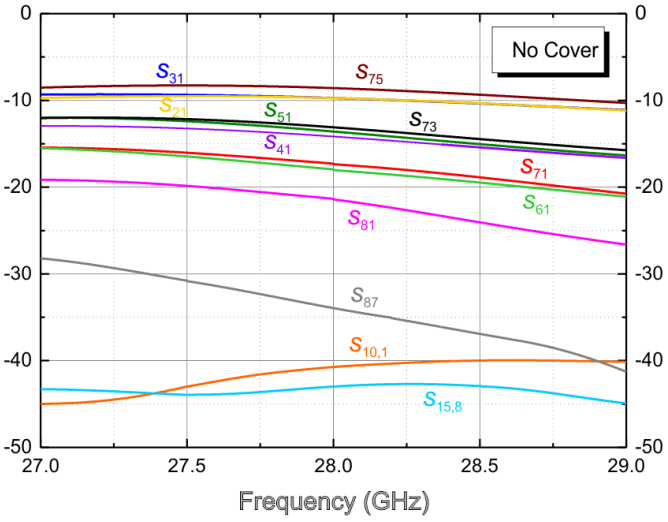

Fig. 8. Magnitudes of the couplings (i.e., magnitudes of S_{jk} parameters, in dB) between some of the ports, for the No cover model.

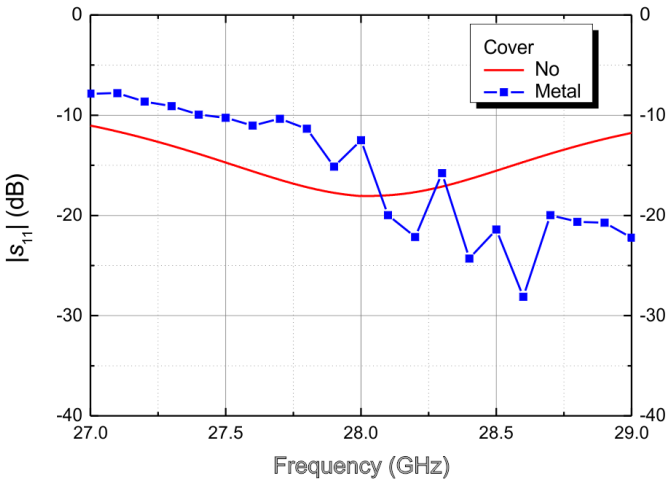

Fig. 9. Magnitudes of the reflection coefficients at the port 1, comparison between No cover and Metal cover models.

Putting metal covers on the frame makes significant difference. The structure becomes highly resonant, which can be seen in comparison with the No cover models. Magnitudes of the reflection coefficients for No cover and Metal cover models are compared in Fig. 9 (at port 1) and Fig. 10 (at port 7). Magnitudes of the couplings between ports 1 and 2, that is, ports 15 and 8 are compared in Fig. 11. Curves for the Metal cover model show high oscillations, which would be even higher if the curves were calculated in more frequency points. Generally, the Metal cover antenna will work, but there is a chance of misfunctioning at some frequencies.

Radiation pattern (Realized gain, in dB) when only generator 1, or 3, is turn on is shown in Fig. 12 (*xz*–plane), and Fig. 13 (*yz*–plane). Because of the symmetry, we can look only antennas 1, 3, 5, and 7. They have somewhat different radiation patterns, as illustrated for antennas 1 and 3. Maximal realized gain for Metal cover fluctuates more, because of the fluctuations in the reflection coefficient.

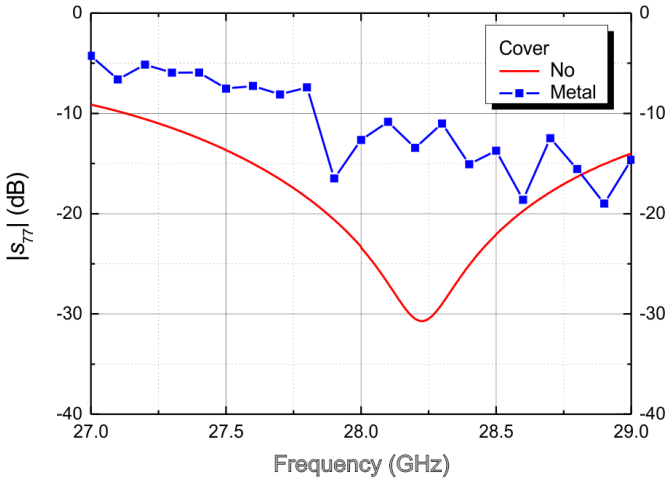

Fig. 10. Magnitudes of the reflection coefficients at the port 7, comparison between No cover and Metal cover models.

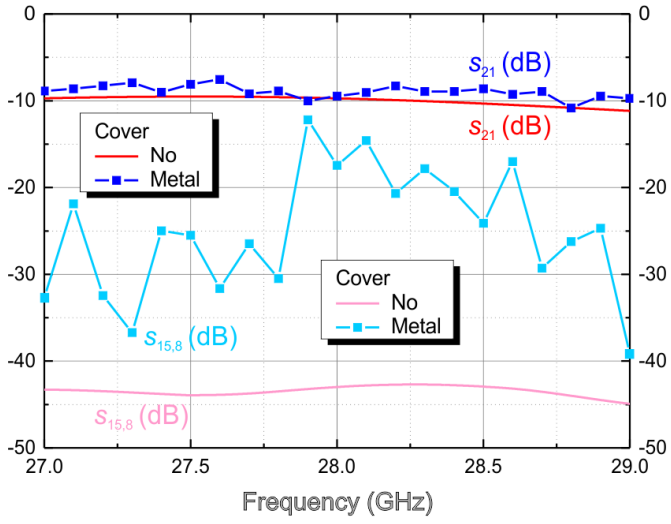

Fig. 11. Magnitudes of the couplings between some ports, comparison between No cover and Metal cover models.

Realized gain can reach as high as 9 dB for the Metal cover model, in the *xz*–plane. Maximal realized gain in the *yz*–plane is about 6 dB.

Finally, we should check the beam steering capability of the phased array. By using elementary mathematical relations for the antenna arrays (wavelength at 28 GHz, the distance between array elements, and the number of elements), we can conclude that only by phase shift between currents of the elements, we can form the beam with the angle with respect to the axes of the array (*x*–axes) between 60 degrees and 90 degrees (90 degrees corresponds to zero phase shift). For this purpose, we used the model with only one eight–element phased array (antennas 1 to 8).

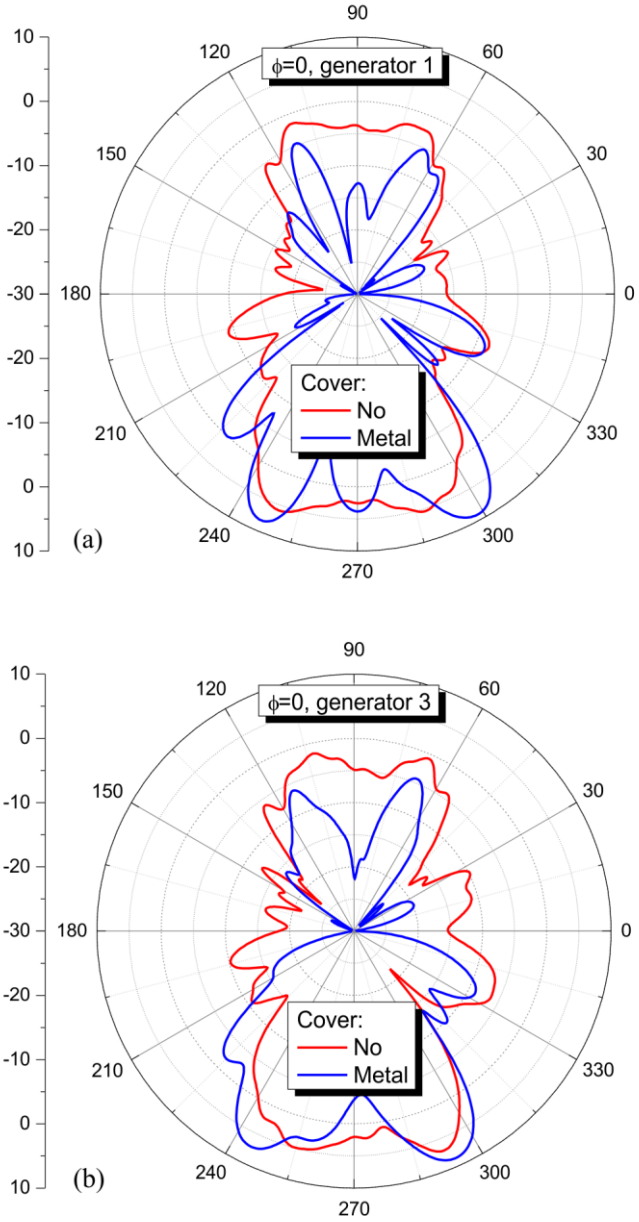

Fig. 12. Radiation pattern (Realized gain, in dB) in the *xz*–plane (ϕ = 0 degrees); comparison between No cover and Metal cover models, when only generator: (a) 1 and (b) 3 is turned on.

Second phased array (antennas 9 to 16) was removed from the model. Technically, by removing the second array, we obtain a different model. However, numerical results show that, for the No cover model, results for radiation patterns of these two models are very similar.

Hence, using the No cover model with the second array removed, we applied only uniform phase shifts to antenna generators, in order to obtain angles (with respect to the *x*–axes) of 90 degrees (no phase shift), 75 degrees, 60 degrees, and 45 degrees. The results for 3D radiation patterns (Realized gain, in dB) are shown in Figs. 14 to 17 (the frame of the handset, shown in the figures, is represented with a mesh of quadrilateral patches).

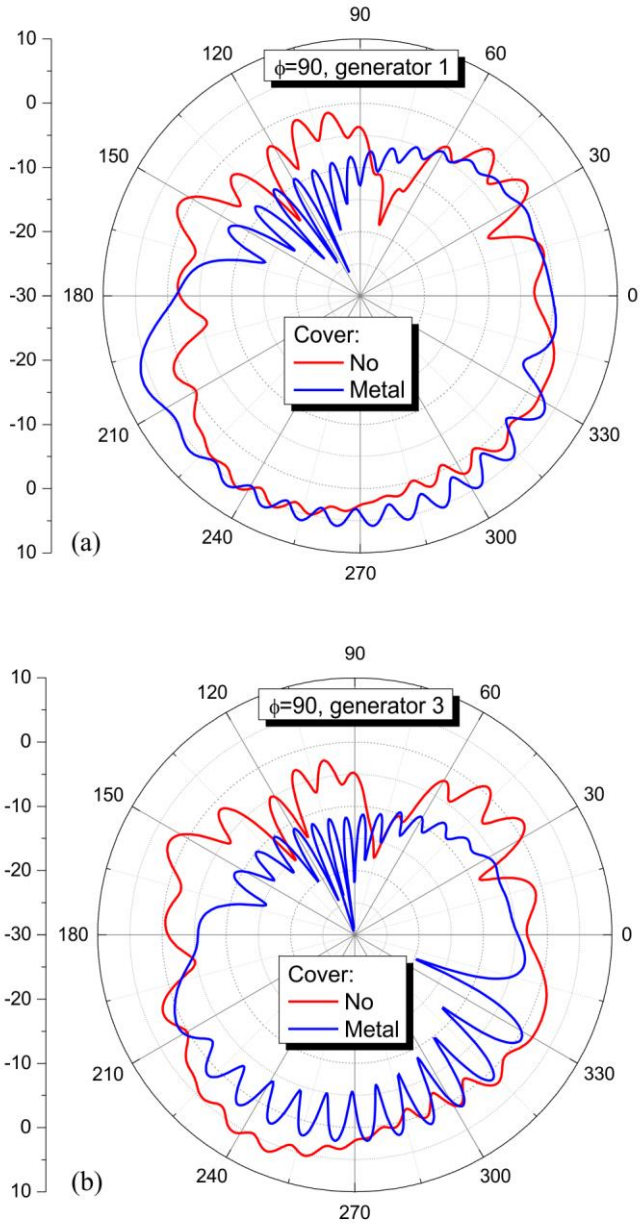

Fig. 13. Radiation pattern (Realized gain, in dB) in the *yz*–plane ($\phi = 90$ degrees); comparison between No cover and Metal cover models, when only generator: (a) 1 and (b) 3 is turned on.

We can see that such setup works correctly for 90 degrees (Fig. 14, maximal realized gain 15.33 dB), 75 degrees (Fig. 15, maximal realized gain 15.89 dB), and 60 degrees (Fig. 16, maximal realized gain 15.47 dB). However, as expected, directivity of the radiation pattern significantly decreases for 45 degrees (which is outside the expected range from 60 degrees to 90 degrees). At this angle, the phased array factor "catches" maximums in two directions (45 degrees is one of them), so the resulting radiation pattern is less directive, and the maximal realized gain is only 9.08 dB (Fig. 17). Technically, for larger scanning range, the smaller distance between array elements (cavities) is needed.

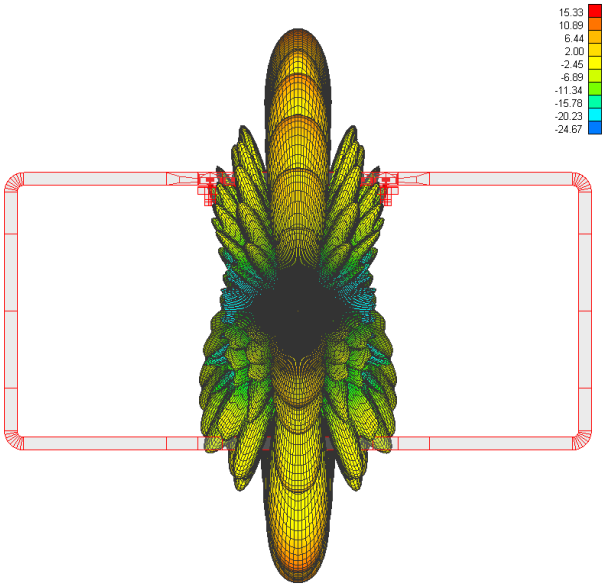

Fig. 14. 3D Radiation pattern (Realized gain, in dB) of the No cover model; phase shift adjusted for 90 degrees angle from the horizontal axes.

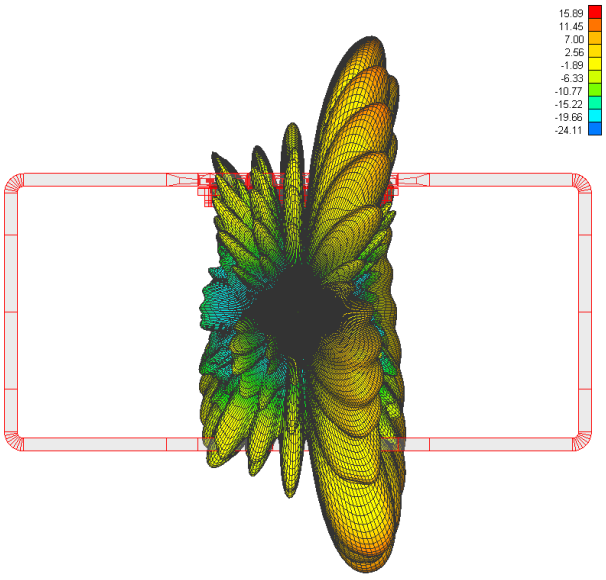

Fig. 15. 3D Radiation pattern (Realized gain, in dB) of the No cover model; phase shift adjusted for 75 degrees angle from the horizontal axes.

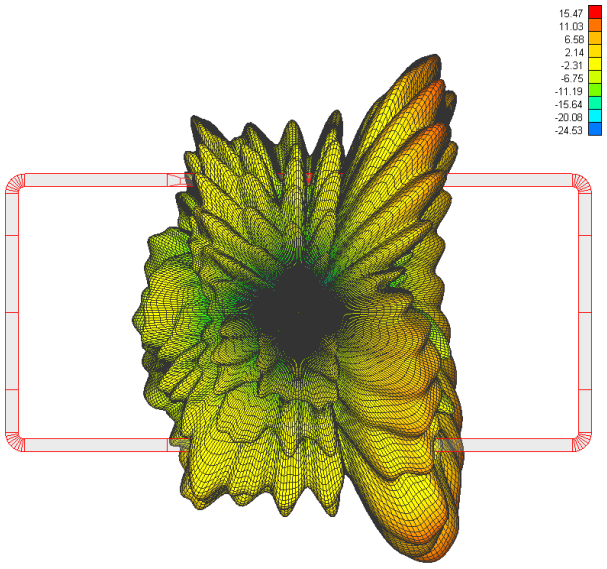

Fig. 16. 3D Radiation pattern (Realized gain, in dB) of the No cover model; phase shift adjusted for 60 degrees angle from the horizontal axes.

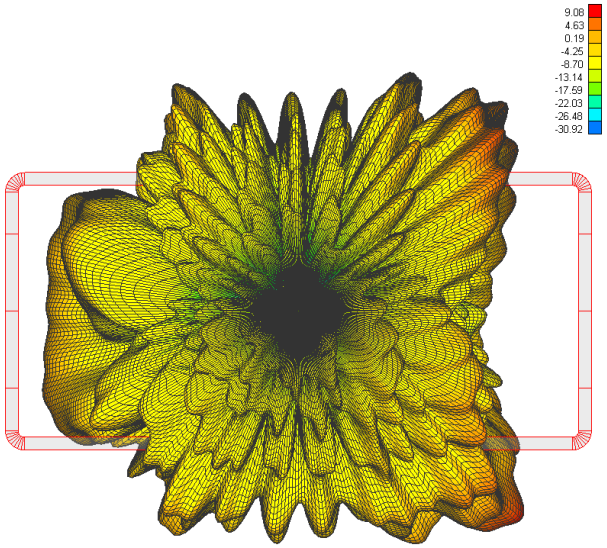

Fig. 17. 3D Radiation pattern (Realized gain, in dB) of No cover model; phase shift adjusted for 45 degrees angle from the horizontal axes.

IV. Conclusions

Numerical simulations show that phased arrays of cavity–backed antennas, in the frequency range around 28 GHz, can be successfully integrated into the metal frame of a cellular handset. If the frame is not covered with metallic plates, the phased array works correctly, within expectations, with large impedance bandwidth and good radiation pattern. However, the key advantage of the cavity–backed antennas is their potential usage in the handsets with fully metallic casing (of course, with slots for camera lenses). By covering the handset frame with the metal plates, S–parameters degrade, with moderate to high oscillations in the frequency range of interest (27 GHz to 29 GHz). These oscillations can result in reduced realized gain and high coupling between antennas, which could cause misfunctioning of the antenna system. Investigated solution has rather small scanning range (for both frame and full metal model), which can be improved by using smaller distance between cavity–backed antennas (and, consequently, smaller cavities). Position of the phased array should be reconsidered.

References

[1] A. I. Sulyman, A. T. Nassar, M. K. Samimi, G. R. Maccartney, T. S. Rappaport and A. Alsanie, "Radio propagation path loss models for 5G cellular networks in the 28 GHZ and 38 GHZ millimeter-wave bands," in IEEE Communications Magazine, vol. 52, no. 9, pp. 78-86, September 2014.

[2] T. S. Rappaport et al., "Millimeter Wave Mobile Communications for 5G Cellular: It Will Work!," in IEEE Access, vol. 1, pp. 335-349, 2013.

[3] W. Hong, K. Baek and S. Ko, "Millimeter-Wave 5G Antennas for Smartphones: Overview and Experimental Demonstration," in IEEE Transactions on Antennas and Propagation, vol. 65, no. 12, pp. 6250-6261, Dec. 2017.

[4] B. Yu, K. Yang, C. Sim and G. Yang, "A Novel 28 GHz Beam Steering Array for 5G Mobile Device With Metallic Casing Application," in IEEE Transactions on Antennas and Propagation, vol. 66, no. 1, pp. 462-466, Jan. 2018.

[5] J. Bang and J. Choi, "A SAR Reduced mm-Wave Beam-Steerable Array Antenna With Dual-Mode Operation for Fully Metal-Covered 5G Cellular Handsets," in IEEE Antennas and Wireless Propagation Letters, vol. 17, no. 6, pp. 1118-1122, June 2018.

[6] S. Long, "Experimental study of the impedance of cavity-backed slot antennas," in IEEE Transactions on Antennas and Propagation, vol. 23, no. 1, pp. 1-7, January 1975.

[7] WIPL-D Pro v17—3D EM Solver, Belgrade, Serbia, 2019, [online] Available: http://www.wipl-d.com